In-Situ Infrared Spectroscopy and Density Functional Theory Modeling of Hafnium Alkylamine Adsorption on Si−OH and Si−H Surfaces

M. Jason Kelly,[†] Joseph H. Han,[‡] Charles B. Musgrave,[‡] and Gregory N. Parsons*[,†]

Department of Chemical and Biomolecular Engineering, North Carolina State University, Raleigh, North Carolina 27695, and Department of Chemical Engineering, Stanford University, Stanford, California 94305

Received May 18, 2005. Revised Manuscript Received July 29, 2005

In-situ attenuated total internal reflection infrared spectroscopy has been used to examine initial adsorption and reaction steps in atomic layer deposition of HfO_2 from tetrakis(diethylamino) hafnium (TDEAHf) on SiO_2 and hydrogen-terminated Si(100) surfaces. At low deposition temperatures (25−250 °C), TDEAHf directly reacts with the Si−H surface, resulting in partial removal of Si−H bonds and formation of a four-membered Si−O−Hf−Si bonding structure that can rapidly oxidize. The hydrogen removal process is observed to continue through many cycles of TDEAHf/H_2O exposure, signifying continued reactivity of the Hf precursor with the silicon surface. Density functional theory calculations have been performed for various reactions between tetrakis(dimethylamino) hafnium and Si−H surfaces, and several possible reaction pathways for hydrogen removal have been identified and analyzed. The calculations suggest that hydrogen removal proceeds by H abstraction by an amine ligand of the Hf precursor and that the abstraction reaction is made more facile by the presence of OH on the otherwise H-terminated Si surface.

I. Introduction

Techniques to experimentally observe and analyze fundamental reaction mechanisms during deposition of advanced dielectric materials on silicon surfaces are important to help direct reactions and achieve well-controlled bonding at dielectric/semiconductor interfaces.[1] In typical processes for deposition of high dielectric constant (high-κ) insulators on silicon, an oxide or nitride interface layer is usually formed at the dielectric/semiconductor interface either intentionally before deposition (to control nucleation and interfacial reaction) or as a reaction byproduct during film deposition. This interfacial layer influences interface defect density and reduces the gate capacitance, limiting reduction of the equivalent oxide thickness. Atomic layer deposition (ALD) is an attractive method for forming ultrathin gate stacks because, in principle, well-controlled sequential reactions in ALD allow the desired film composition and structure to be achieved.[2,3] Several groups have reported the effects of various surface pretreatments, including hydrogen termination, on atomic layer deposition of high-κ dielectrics.[3−7] Hydrogen termination of the silicon surface significantly inhibits dielectric film growth during the initial ALD cycles[4−6] resulting in poorly controlled interface structures. In-situ infrared absorption has been used to study detailed reactions between trimethyl aluminum (TMA) and hydrogen-terminated silicon surfaces.[8,9] Results demonstrate a direct reaction between Si−H and TMA, resulting in Si−Al−$(CH_3)_2$ surface units. It is suggested that upon exposure to water vapor, these surface species promote subsurface silicon oxidation and formation of a silicon oxide interface layer. These results have been used to suggest Al-methyl groups as an alternate surface passivation approach for ALD of other dielectrics, including HfO_2. Ab initio calculations[10] show that the reaction between TMA and the Si−H surface forms Si−Al−$(CH_3)_2$ and CH_4 as products and is exothermic overall, with a reaction barrier of ∼28 kcal/mol. TMA is a very reactive precursor, where, for example, it can react directly with siloxane bridges on SiO_2 surfaces with no Si−OH

* Author to whom correspondence should be addressed. E-mail: parsons@ncsu.edu.
[†] North Carolina State University.
[‡] Stanford University.

(1) Murto, R. W.; Gardner, M. I.; Brown, G. A.; Zeitzoff, P. M.; Huff, H. R. *Solid State Technol.* **2003**, 43−48.
(2) Ritala, M.; Leskela, M. In *Handbook of Thin Film Materials*; Nalwa, H. S., Ed.; Academic Press: New York, 2001; Vol. 1, Chapter 2.
(3) Hausmann, D.; Kim, E.; Becker, J.; Gordon, R. G. *Chem. Mater.* **2002**, *14*, 4350−4358.
(4) Green, M. L.; Ho, M. Y.; Busch, B.; Wilk, G. D.; Sorsch, T.; Conard, T.; Brijs, B.; Vandervorst, W.; Raisanen, P. I.; Muller, D.; Bude, M.; Grazul, J. *J. Appl. Phys.* **2002**, *92*, 7168−7174.
(5) Triyoso, D. H.; Hegde, R. I.; Grant, J.; Fejes, P.; Liu, R.; Roan, D.; Ramon, M.; Werho, D.; Rai, R.; La, L. B.; Baker, J.; Garza, C.; Guenther, T.; White, B. E.; Tobin, P. J. *J. Vac. Sci. Technol., B* **2004**, *22*, 2121−2127.
(6) Puurunen, R. L.; Vandervorst, W.; Besling, W. F. A.; Richard, O.; Bender, H.; Conard, T.; Zhao, C.; Delabie, A.; Caymax, M.; De Gendt, S.; Heyns, M.; Viitanen, M. M.; de Ridder, M.; Brongersma, H. H.; Tamminga, Y.; Dao, T.; de Win, T.; Verheijen, M.; Kaiser, M.; Tuominen, M. *J. Appl. Phys.* **2004**, *96*, 4878−4889.
(7) Duenas, S.; Castan, H.; Garcia, H.; Barbolla, J.; Kukli, K.; Ritala, M.; Leskela, M. *Thin Solid Films* **2004**, *474*, 222−229.
(8) Frank, M. M.; Chabal, Y. J.; Wilk, G. D. *Appl. Phys. Lett.* **2003**, *82*, 4758−4760.
(9) Frank, M. M.; Chabal, Y. J.; Green, M. L.; Delabie, A.; Brijs, B.; Wilk, G. D.; Ho, M. Y.; da Rosa, E. B. O.; Baumvol, I. J. R.; Stedile, F. C. *Appl. Phys. Lett.* **2003**, *83*, 740−742.
(10) Halls, M. D.; Raghavachari, K.; Frank, M. M.; Chabal, Y. J. *Phys. Rev. B* **2003**, *68*.

10.1021/cm051064h CCC: $30.25
Published on Web 09/28/2005

present.[11] Reactions between metal-containing precursors and silicon surfaces are of interest to enable control over dielectric/silicon interface structure, and here we investigate the case of hafnium alkylamine reactions with Si−OH and Si−H surfaces.

Metal−alkylamine precursors are of interest as precursors for ALD because they do not involve halogen atoms, and many are liquids at room temperature or have low melting points. Furthermore, alkylamines are generally more easily oxidized than metal alkoxides because metal−nitrogen bonds are usually weaker, and therefore more easily broken, than the metal−oxygen bonds in alkoxides. Similarly, alkylamines are generally more stable than metal alkyls, providing a balance between reactivity and stability in processing.[3,12] This article presents a study of reaction mechanisms in insulator deposition by ALD on hydrogen-terminated and preoxidized silicon surfaces. Of particular interest are the mechanisms associated with atomic layer deposition of hafnium oxide from hafnium ethylamine precursors onto a hydrogen-terminated silicon (100) surface. The goal is to better understand the initial reaction sequences in HfO_2 deposition that can help enable the fabrication of well-controlled, atomically abrupt silicon/metal−oxide interfaces.

II. Experimental Methods

In this article, initial adsorption of tetrakis(diethylamino) hafnium on SiO_2 and hydrogen-terminated Si surfaces is characterized using in-situ attenuated total internal reflection Fourier transform infrared spectroscopy (ATR-FTIR). In this approach,[13] infrared radiation is focused through KBr reactor windows onto the beveled edge of a high resistivity silicon wafer resulting in total internal reflection and propagation of the radiation along the wafer. Upon exiting the wafer, the photon flux is directed by a parabolic mirror to a HgCdTe IR detector cooled with liquid N_2. The IR bench, beam path, and external detector are all enclosed and flushed with a continuous flow of dry air. Species adsorbed on the silicon surface will interact with and absorb the evanescent IR wave directed along the surface normal. Comparing the IR signal before and after surface adsorption steps allows the vibrational properties of the adsorbed species to be observed. A schematic of the reactor setup used for the experiment (base pressure $\sim 2 \times 10^{-7}$ Torr) is shown in Figure 1. The chamber is equipped with a plasma generation source to study effects of surface plasma exposure. The liquid precursor flux is introduced from a heated vessel through an ultrahigh vacuum leak valve. Before beginning experiments, the precursor vessel is cooled and pumped through a bypass line to help remove volatile impurities. For the geometry used, the IR signal interacts with the front surface of the ATR crystal approximately 40 times as it progresses through the 40-mm wafer. Because of oxygen impurities and silicon multiphonon modes in the Si ATR crystal, the IR signal is absorbed at energies below ~ 1500 cm^{-1}. The instrument therefore allows analysis between ~ 4000 cm^{-1} and 1500 cm^{-1}, which is sufficient for a large number of vibrational modes of interest in metal−organic/Si reactions, including C−H (2800−3100 cm^{-1}), Si−H (2000−2200 cm^{-1}), N−H (3400−3500 cm^{-1}), OH (3500−3900 cm^{-1}), and others. This approach is sensitive to in-plane and out-of-plane vibrations of the adsorbate species. Polarization was not used for the work reported here, and all spectra shown are referenced to a spectrum of the starting surface without any further correction or baseline subtraction unless specifically noted. Figure 2a shows a spectrum from an octadecyltrichlorosilane (OTS) self-assembled monolayer measured on an oxidized silicon ATR crystal in this system. Features associated with carbon−hydrogen stretches on methyl and methylene groups are observed. Figure 2b shows the total single-beam signal through the ATR crystal as a function of substrate temperature. The signal decreases somewhat between room temperature and 175 °C, but at higher temperatures, thermal free-carrier generation increases the IR scattering, and at 300 °C, the signal is attenuated by >50%. The temperature range for experiments is limited to about 300 °C. At elevated temperature (200−250 °C), the system was stable, and transmission signal intensity was very reproducible.

The starting surfaces of Si(100) ATR crystals were prepared in air by thermal or wet-chemical treatment before each exposure sequence and were loaded into the system within 10 min of preparation. Several pretreatment approaches were studied, including chemical surface oxidation to produce 5 Å hydroxyl-rich SiO_2[4]

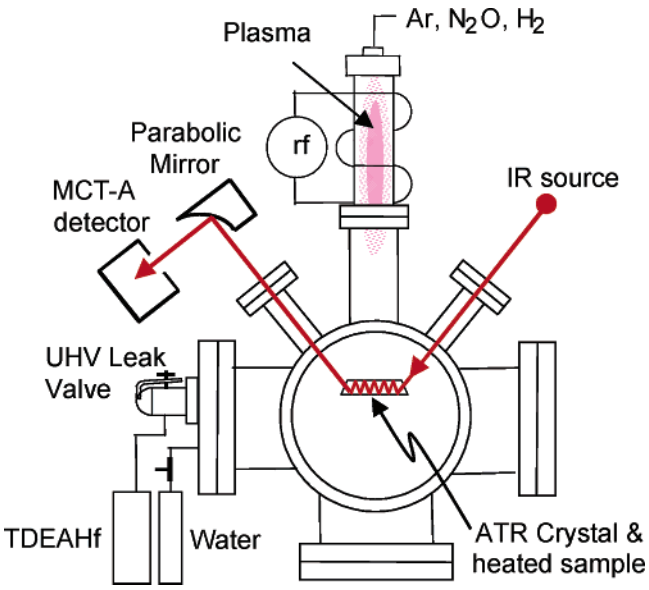

Figure 1. Schematic of the attenuated total internal reflection FTIR system and reactor geometry used for in-situ spectroscopy.

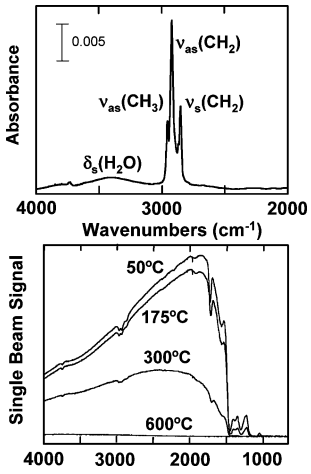

Figure 2. (a) Attenuated total internal reflectance infrared absorbance spectrum for a reference octadecyl trichlorosilane monolayer on thin thermal SiO_2. The thermal oxide was used as the reference spectrum. (b) Single beam spectra showing effect of temperature on IR transmission through an ATR silicon substrate with thermal oxide.

(11) Puurunen, R. L.; Root, A.; Sarv, P.; Haukka, S.; Iiskola, E. I.; Lindblad, M.; Krause, A. O. I. *Appl. Surf. Sci.* **2000**, *165*, 193−202.
(12) Cardin, D. J.; Lappert, M. F.; Raston, C. L. *Chemistry of Organo-Zirconium and -Hafnium Compounds*; Ellis Horwood Limited: West Sussex, U.K., 1986.
(13) Chabal, Y. J. *Surf. Sci. Rep.* **1988**, *8*, 211−357.

(following the common RCA oxidation process: aqueous H_2O_2/NH_4OH at 45 °C) and silicon/hydrogen termination by thermal oxidation at 900 °C to produce ~30 Å sacrificial oxide followed by surface etching in dilute HF acid solution. Thermal SiO_2 surfaces were also prepared by oxidation of HF-last surfaces in air at 900 °C for 3 min. Tetrakis(diethylamino) hafnium [$Hf(N(C_2H_5)_2)_4$] (TDEAHf) was used as the source for hafnium. The precursor is generally kept at room temperature and then is heated to 65°C for the experiment.

The reaction sequence involved (i) preparing the ATR wafer surface by external wet chemical treatment and placing the surface in a vacuum system to pump to the $10^{-6}-10^{-7}$ Torr range; (ii) comparing the IR signal from the clean surface to a reference wafer to confirm surface cleanliness; (iii) heating the sample and allowing 30 min for the temperature to equilibrate; and (iv) introducing precursor to the reaction chamber and monitoring pressure and IR signal as a function of time. The total reactant exposure in Langmuirs was estimated for each spectrum collected, and a range of surface exposures between 10^3 and 10^7 Langmuirs (1 L = 10^{-6} Torr-sec) was investigated. Typical exposure pressure was in the 1−10 mTorr range. Exposure flux and the signal to noise in the spectroscopy system are sufficient to enable reproducible data set acquisition at approximately 30-s intervals. For the spectra shown here, the chamber was evacuated before each measurement, and typically 512 or 1024 scans were collected at 4 cm^{-1} resolution, corresponding to a data collection time of ~10−20 min per spectrum. Substrate temperature was fixed between room temperature and ~250 °C, and IR spectra were collected at the substrate temperature. After precursor exposure, the reaction sequence concluded with (v) evacuating the system and then repeating the exposure and measurement procedure using the water vapor reactant.

III. Theoretical Methods

The theoretical analysis was based on quantum chemical calculations using the B3LYP hybrid density functional theory (DFT) method[14,15] and a mixed Gaussian basis set. For computational efficiency, simulations were performed using the dimethyl precursor, which has similar reactivity and spectroscopic properties to the diethyl species, except that it precludes beta-hydride elimination and, for example, C−C stretching modes. Hf and Si atoms are described using the Los Alamos LANL2 effective core potential (ECP) and a valence double-ζ basis set.[16−21] Previous calibration studies have shown that polarization functions on first-row atoms are critical to obtaining accurate energies;[22] as such, the D95-(d,p)[23] basis set was applied to all H, C, N, and O atoms including the OH* and H* surface species and $Hf[N(CH_3)_2]_4$ ligands. The * denotes surface groups as opposed to the atoms used to terminate the subsurface atoms. We optimize the molecular geometries to locate stationary points and perform frequency calculations at these geometries to predict the vibrational signatures of each structure, to verify the nature of the stationary points, to calculate zero-point energy corrections, and to construct the associated partition functions from which thermochemical properties are calculated. For the frequency calculations, the hydrogen atoms that terminate the subsurface silicon atoms were given a mass of 1000.0 amu to decouple those vibrational modes from the ones generated by surface Si−H* species. All calculations are performed using GAUSSIAN 98.[24] The default convergence criteria were applied, and the calculated frequencies that are presented have not been scaled.

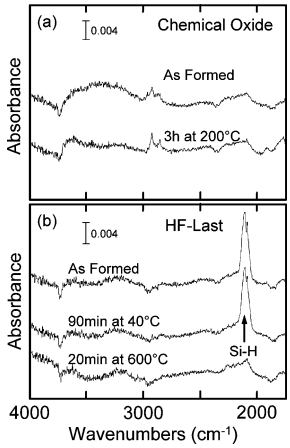

Figure 3. Infrared signal for (a) chemical oxide and (b) HF-last Si(100) surfaces. The spectra are referenced to a thermally oxidized silicon crystal and are baseline corrected to minimize shifts resulting from optical mismatch between the sample and background crystals. The negative-going feature at 3740 cm^{-1} is from variations in H_2O in the beam path within the spectrometer.

IV. Experimental Results

A. Analysis of Starting Surfaces. Figure 3 shows the infrared signal for the as-prepared chemical oxide and HF-last surfaces. Spectra are shown as acquired immediately after placing the substrates in the chamber and after heating and vacuum exposure. The background spectra for these spectra were obtained from a thermally oxidized silicon wafer. For the chemical oxide, shown in Figure 3a, broad features consistent with a high density of associated hydroxyl surface groups (3000−3800 cm^{-1}) are observed, and the intensity of the OH modes decreases upon vacuum anneal for 3 h at 200 °C. Some C−H modes are also observed, which are likely due to organic adsorption during sample transfer in ambient. For the precursor adsorption studies described below at 200 °C, a large fraction of surface hydroxyl groups will

(14) Becke, A. D. *J. Chem. Phys.* **1993**, *98*, 1372−1377.
(15) Becke, A. D. *J. Chem. Phys.* **1993**, *98*, 5648−5652.
(16) Hay, P. J.; Wadt, W. R. *J. Chem. Phys.* **1985**, *82*, 270−283.
(17) Hay, P. J.; Wadt, W. R. *J. Chem. Phys.* **1985**, *82*, 284−298.
(18) Hay, P. J.; Wadt, W. R. *J. Chem. Phys.* **1985**, *82*, 299−310.
(19) Hay, P. J.; Wadt, W. R. *J. Chem. Phys.* **1985**, *82*, 270−283.
(20) Hay, P. J.; Wadt, W. R. *J. Chem. Phys.* **1985**, *82*, 299−310.
(21) Wadt, W. R.; Hay, P. J. *J. Chem. Phys.* **1985**, *82*, 284−298.
(22) Han, J. H.; Gao, G.; Widjaja, Y.; Garfunkel, E.; Musgrave, C. B. *Surf. Sci.* **2003**, *550*, 199−212.
(23) Dunning, T. H., Jr.; Hay, P. J. In *Modern Theoretical Chemistry*; Schaefer, H. F., III, Ed.; Plenum: New York, 1976; pp 1−28.
(24) Frisch, M. J.; Trucks, G. W.; Schlegel, H. B.; Scuseria, G. E.; Robb, M. A.; Cheeseman, J. R.; Zakrzewski, V. G.; Montgomery, J. A., Jr.; Stratmann, R. E.; Burant, J. C.; Dapprich, S.; Millam, J. M.; Daniels, A. D.; Kudin, K. N.; Strain, M. C.; Farkas, O.; Tomasi, J.; Barone, V.; Cossi, M.; Cammi, R.; Mennucci, B.; Pomelli, C.; Adamo, C.; Clifford, S.; Ochterski, J.; Petersson, G. A.; Ayala, P. Y.; Cui, Q.; Morokuma, K.; Rega, N.; Salvador, P.; Dannenberg, J. J.; Malick, D. K.; Rabuck, A. D.; Raghavachari, K.; Foresman, J. B.; Cioslowski, J.; Ortiz, J. V.; Baboul, A. G.; Stefanov, B. B.; Liu, G.; Liashenko, A.; Piskorz, P.; Komaromi, I.; Gomperts, R.; Martin, R. L.; Fox, D. J.; Keith, T.; Al-Laham, M. A.; Peng, C. Y.; Nanayakkara, A.; Challacombe, M.; Gill, P. M. W.; Johnson, B.; Chen, W.; Wong, M. W.; Andres, J. L.; Gonzalez, C.; Head-Gordon, M.; Replogle, E. S.; Pople, J. A. *Gaussian 98*, Revision A.11.2; Gaussian, Inc.: Pittsburgh, PA, 2001.

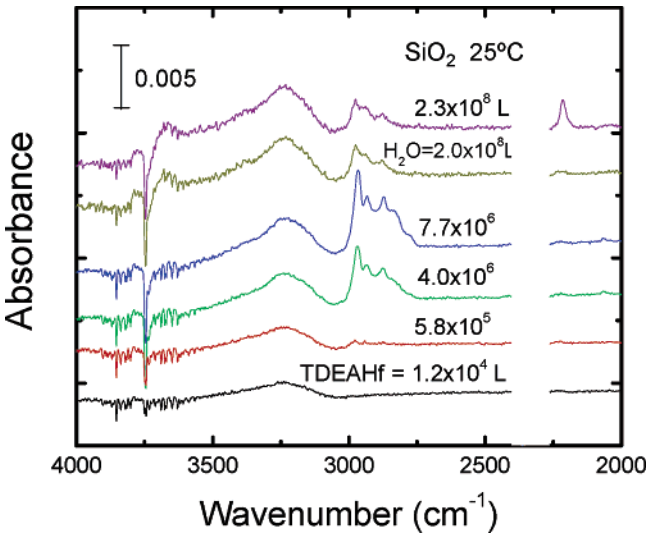

Figure 4. ATR−FTIR absorbance after various exposures of the SiO_2 surface to TDEAHf at room temperature. Measurements were performed after evacuation of the precursor from the chamber, and typical scan conditions were 1024 scans at 4 cm^{-1} resolution. The CH mode intensity is observed to increase with exposure, and subsequent exposure to H_2O results in a decrease in CH modes, consistent with ligand oxidation. Spectra are referenced to the SiO_2 starting surface.

remain. For the HF-last surface, shown in Figure 3b, Si−H stretching modes are observed, consistent with a typical rough and faceted hydrogen-terminated Si(100) surface.[25] Some absorption due to hydroxyl groups may also be present. The surface hydrogen is stable upon a 90-min anneal at 40 °C, but the hydrogen desorbs upon annealing at 600 °C for 20 min.

B. TDEAHf Exposure on SiO_2. Figure 4 shows infrared spectra collected as a function of TDEAHf exposure at room temperature on the thermally oxidized silicon surface. The bottom spectrum corresponds to a 1.2×10^4 L TDEAHf exposure, and spectra for progressively increasing exposure are also shown. The top two spectra were collected after the surface was exposed to water vapor. All the spectra in Figure 4 show several characteristic features, including modes at ~2970, 2930, 2870, and 2830 cm^{-1} and a shoulder near 2775 cm^{-1}. The features between 2830 and 2970 cm^{-1} are consistent with symmetric and asymmetric methyl (CH_3) and methylene (CH_2) stretches of a surface-bound Hf-diethylamine ligand. Features are also expected to arise from charge-induced frequency lowering of the primary C−H mode because of interaction with the neighboring N lone pair,[26,27] giving rise to additional structure (i.e., Bohlmann band) in the C−H stretch spectrum. Several sharp modes from ~3600 to 3900 cm^{-1} are related to vapor-phase water and CO_2 in the beam path, and data in this range is removed from the figures. A strong doublet at 2340/2360 cm^{-1} is also observed because of CO_2 in the beam path. A broad mode near 3200 cm^{-1} is assigned to N−H modes related to adsorption or reaction on the KBr reactor windows. Pumping on the chamber at $<10^{-6}$ Torr for several hours resulted in selective loss of the 3200 cm^{-1} mode. On the oxide surface, the intensity of the C−H modes is observed to increase with exposure time and a plot of total absorbance versus exposure follows first-order Langmuir kinetics: $(1 - \theta) = \exp[-(J \cdot t)/n_o\zeta]$ where θ is the surface coverage fraction, $(J \cdot t)$ is the surface precursor exposure, n_o is the density of surface sites for adsorption, and ζ is the chemisorption reaction probability. Comparison of the integrated absorbance in the C−H stretching regime of the OTS monolayer in Figure 2 with the C−H absorbance from the adsorbed precursor after 7.7×10^6 L exposure in Figure 4 results in an absorbance ratio $[\int(A_{TDEAHf})\partial\omega/\int(A_{OTS})\,\partial\omega]$ of ~0.43. Extracting quantitative comparisons of molecular surface coverage from the relative integrated mode strengths of these different molecules is difficult because of expected differences in mode strengths and uncertainty in the number and nature of ligands remaining on the adsorbed precursor, but the magnitude of the absorbance ratio is only slightly larger (by a factor of ~1.2) than what would be expected for monolayer coverage for TDEAHf with two diethylamino ligands and a smaller molecular surface density for TDEAHf relative to OTS. The exposure of $\sim 8 \times 10^6$ L observed for saturation is larger than expected for typical ALD processing, and the fit to Langmuirian kinetics results in a small chemisorption reaction probability ($\sim 3 \times 10^{-7}$). A reaction probability near 0.5 has been observed[28] for titanium alkylamide (tetrakis dimethylamino titanium, TDMAT) exposure on SiO_2, and a large difference in adsorption probability between TDMAT and TDEAHf is not necessarily expected. Rapid oxidation of adsorbed precursor could, for example, reduce the surface ligand concentration, or surface impurities that act to block adsorption could reduce surface reaction probability. Organic impurities on the starting surface are observed in the IR data in Figure 3, and the ratio of integrated absorbance of the C−H related impurities to that for the OTS layer in Figure 2 is ~0.1.

After exposing the chemisorbed precursor to 2×10^8 L of H_2O, the C−H related modes are observed to decrease, but they are not completely removed. We also observe the appearance of a broad mode near 3700 cm^{-1}, consistent with precursor oxidation and formation of surface OH groups. With continuing exposure to H_2O, a mode is observed to appear near 2220 cm^{-1}, possibly because of surface carbon−nitrogen stretching modes.

C. TDEAHf Exposure on Hydrogen-Terminated Silicon. Hydrogen-terminated silicon (100) surfaces were also exposed to TDEAHf at room temperature and at 250 °C, and results are shown in Figures 5 and 6. The data in Figure 5 shows IR absorbance after exposing the hydrogen-terminated surface to various doses of TDEAHf at room temperature. The resulting spectra exhibit features similar to those in Figure 4 for room-temperature exposure on the SiO_2 surface, but the C−H mode intensity is smaller on Si−H after nearly similar precursor exposure conditions. A plot of integrated C−H absorbance versus precursor exposure follows the trend of a Langmuir isotherm, where the saturation integrated intensity is approximately 10 times

(25) Chabal, Y. J.; Higashi, G. S.; Raghavachari, K.; Burrows, V. A. *J. Vac. Sci. Technol., A* **1989**, *7*, 2104−2109.
(26) Mui, C.; Wang, G. T.; Bent, S. F.; Musgrave, C. B. *J. Chem. Phys.* **2001**, *114*, 10170−10180.
(27) McKean, D. C.; Ellis, I. A. *J. Mol. Struct.* **1975**, *29*, 81.
(28) Killampalli, A. S.; Ma, P. F.; Engstrom, J. R. *J. Am. Chem. Soc.* **2005** (in press).

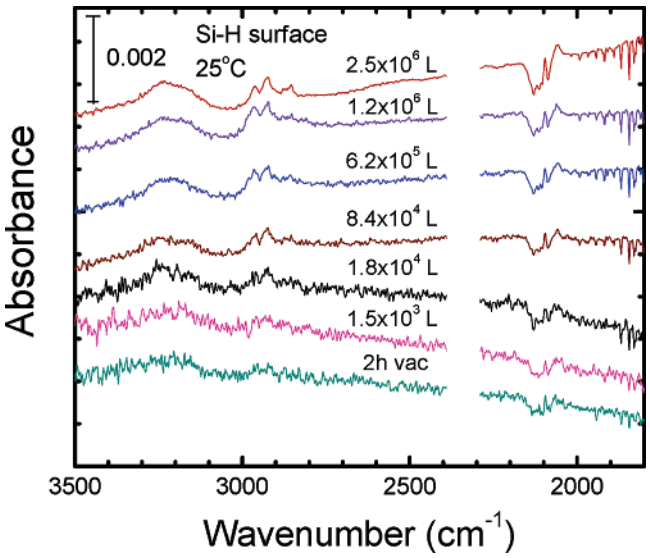

Figure 5. ATR−FTIR absorbance after exposing the hydrogen-terminated surface to various doses of TDEAHf at room temperature. The C−H mode intensity for precursor on Si−H is reduced significantly compared to that on the SiO_2 surface. Reduction in Si−H is observed, consistent with hydrogen abstraction during TDEAHf precursor exposure. All spectra are referenced to the Si−H starting surface.

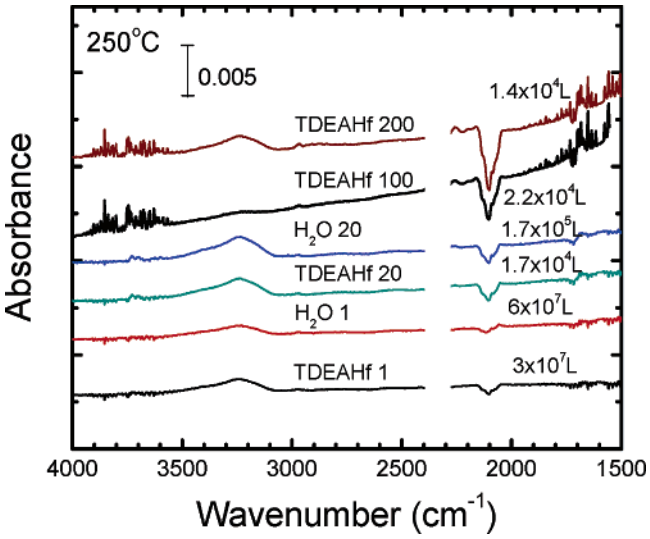

Figure 6. ATR−FTIR spectra after sequential exposure of the Si−H surface to TDEAHf and water over many cycles at a substrate temperature of 250 °C. The first cycle consisted of long exposures to TDEAHf (3×107 L) and water (6×10^7 L), followed by 200 shorter cycles of $\sim 2 \times 10^4$ L TDEAHf and 2×10^5 L water, respectively. For cycles 1 and 20, results are shown from after each half cycle, whereas for cycles 100 and 200, results only after the TDEAHf exposure step are shown. Spectra are referenced to the Si−H surface.

smaller than that observed for adsorption on SiO_2. The spectra in Figure 5 are referenced to the Si−H starting surface, so the negative-going features between 2085 and 2130 cm^{-1} correspond to the removal of Si−H stretching vibrational modes from the surface during exposure. This decrease is ascribed to hydrogen abstraction from Si−H surface bonds during precursor exposure, and proposed mechanisms for this abstraction are described below. The negative-going features in the Si−H stretch region are consistent with removal from SiH_2 and SiH_3 surface units, and a complementary positive-going mode near 2060 cm^{-1} is likely due to formation of monohydride bonds, possibly by abstraction of hydrogen from SiH_2. Comparing the integrated absorbance of the negative-going Si−H mode relative to the Si−H starting surface, the Si−H loss after $\sim 2.5 \times 10^6$ L of TDEAHf exposure at room temperature corresponds to ~10% of the total Si−H originally on the surface. This magnitude of Si−H loss along with the observed submonolayer (~10%) surface coverage of TDEAHf is consistent with a concerted mechanism involving precursor adsorption and Si−H removal. The larger size of the TDEAHf compared to Si−H may suggest loss of multiple Si−H bonds for each precursor molecule adsorbed. However, experimental accuracy makes it difficult to draw detailed quantitative conclusions. Exposing the Si−H surface to the precursor, the C−H mode intensity is observed to follow Langmuir adsorption kinetics, similar to precursor exposure on SiO_2, but the saturation concentration is ~10% of the intensity observed on SiO_2. The slope of the Langmuirian fit also shows a small surface reaction probability ($\sim 10^{-7}$). The smaller uptake of precursor on Si−H versus SiO_2 is consistent with the mechanism and theoretical calculations presented below where precursor adsorption on Si−H occurs primarily on surface sites that are oxidized by water or other oxygen sources present in the reactor system.

Figure 6 shows results of sequential exposure of the Si−H surface to TDEAHf and water over many cycles at a substrate temperature of 250 °C. The first cycle consisted of long exposures to TDEAHf (3×10^7 L) and water (6×10^7 L), followed by 200 shorter cycles of $\sim 2 \times 10^4$ L TDEAHf and 2×10^5 L water, respectively. The figure shows results after each half cycle (i.e., after TDEAHf or H_2O exposure) for cycles 1 and 20, as well as after TDEAHf exposure cycle numbers 100 and 200. In this case, cycle 1 was long exposures (3×10^7 L TDEAHf and 6×10^7 L H_2O) and cycles 2−200 were shorter ($\sim(1-2) \times 10^4$ L TDEAHf and H_2O). After the initial 3×10^7 L TDEAHf exposure at 250 °C, the integrated absorbance of the negative-going Si−H mode is approximately the same as that shown in Figure 5 for 3×10^6 L exposure at room temperature. The results in Figures 5 and 6 consistently show removal of Si−H modes during TDEAHf exposure to be not strongly dependent on substrate temperature. However, the Si−H starting surface is expected to be different at different temperatures, making quantitative comparisons of temperature dependence difficult to interpret. It is interesting to note in Figure 6 that as the Si−H surface is exposed to repeated TDEAHf/H_2O cycles, the intensity of the negative-going Si−H mode continues to increase indicating that hydrogen continues to be removed even after more than 100 TDEAHf/H_2O cycles. Therefore, H removal is not strongly related to exposure for a single cycle, but it continues to increase upon repeated TDEAHf and H_2O exposures. A precursor adsorption and hydrogen abstraction scheme consistent with these results is discussed below. Figure 7 shows X-ray photoelectron spectroscopy data of Si−H and SiO_2 surfaces after exposure to 10 cycles of TDEAHf and H_2O at 250 °C. The XPS measurements were performed with a Riber LAS3000 (MAC2 analyzer, Mg Kα $h\nu = 1253.6$ eV, nonmonochromatic X-ray source) at 75° takeoff angle with 0.1 eV step size, and the adventitious C 1s peak was set to a binding energy of 285.0 eV. The data confirms the presence of Hf and O on both surfaces, with

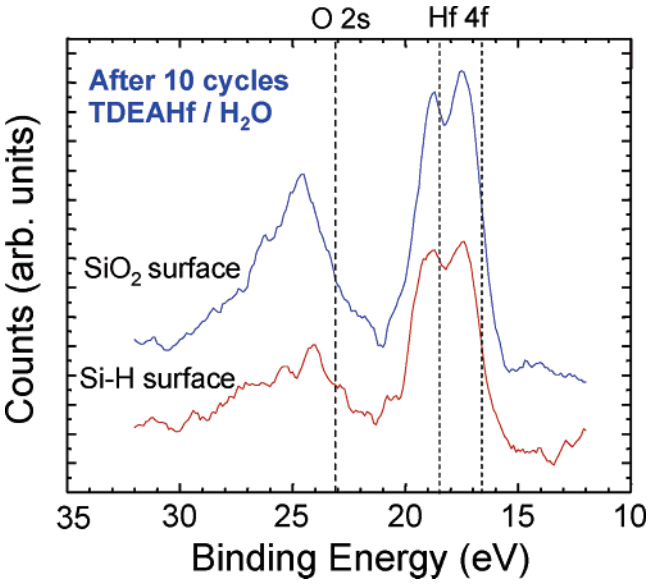

Figure 7. X-ray photoelectron spectra of Si−H and SiO_2 surfaces after exposure to 10 cycles of TDEAHf and H_2O at 250 °C. The data confirms the presence of Hf and O on both surfaces, with somewhat less Hf present on the initially hydrogen-terminated surface. The peak positions are consistent with mixed Si−O and Hf−O bonds in the near surface region.

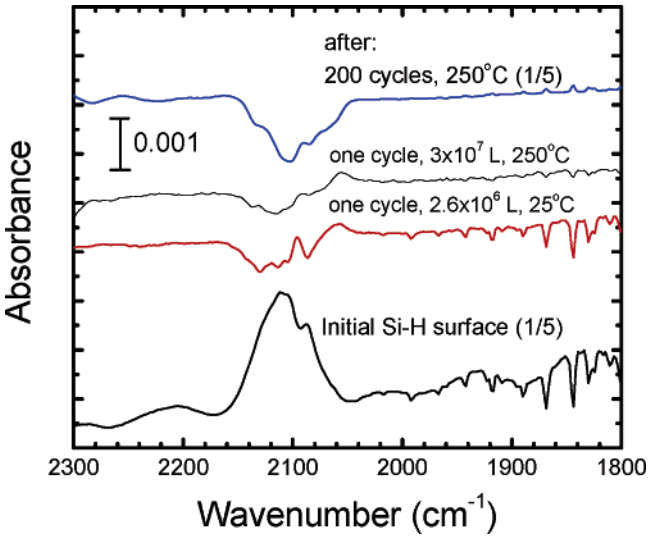

Figure 8. Si−H IR vibrational modes for the initial surface and after various precursor exposure doses at 25 and 250 °C. The spectra for the initial surface and the surface after 200 cycles are reduced in scale by 5× relative to the scale bar. The initial Si−H surface is referenced to a SiO_2 surface, and subsequent spectra are referenced to the initial Si−H spectrum shown. The positive-going shoulder on the low wavenumber side of the Si−H modes suggests a possible shift from higher hydride to monohydride bonding. Longer exposure (top spectrum) indicates eventual removal of these monohydride features.

somewhat less Hf present on the initially hydrogen-terminated surface. The peak positions are consistent with mixed Si−O and Hf−O bonds in the near surface region.

The structures of the Si−H IR vibrational modes for the initial surface and after various exposure doses at 25 and 250 °C are shown in detail in Figure 8. The spectrum of the initial surface shows a broad Si−H mode, consistent with surface roughness and a variety of Si−H, SiH_2, and SiH_3 surface species.[25] After a single long exposure of the Si−H surface to TDEAHf at 25 or 250 °C, the Si−H mode shows a decrease between 2070 and 2150 cm^{-1}, consistent with loss of H from SiH_3 and SiH_2 bonding sites. After the initial precursor exposure dose at 25 and 250 °C, both spectra show a positive-going feature at 2060 cm^{-1} which indicates a change in the local environment for the Si−H vibration. This could result from conversion of the higher hydrides to monohydride (Si−H) units on the surface through hydrogen abstraction, or it may result from a change in one or more of the back-bonds made by the local silicon atom, where charge donation to the silicon can result in a shift of the Si−H frequency to lower wavenumbers. The conversion of higher hydrides to Si−H is consistent with a preference for abstraction of H from SiH_2 and SiH_3 units over monohydride modes on the growth surface. After many cycles at 250 °C (top spectrum in Figure 8), the mode shows a net decrease at 2060 cm^{-1}, indicating the loss of these converted (or otherwise frequency shifted) Si−H bonds.

V. Theoretical Results

The theoretical analysis of hafnium alkylamine adsorption and reaction on SiO_2 and Si−H* surfaces is made complex by the fact that the hydrogen-terminated Si(100) surface explored experimentally has significant atomic-scale surface roughness and faceting, resulting in a wide range of surface hydride modes. Modeling of this rough extended surface using quantum chemical methods is not readily feasible. To theoretically explore the nature of the reaction between hafnium alkylamines and the SiO_2 and Si−H* surfaces, we have used the 2 × 1 reconstructed Si(100) surface with tetrakis(dimethylamino) hafnium (TDMAHf) as a model system and have obtained reaction potential energy surfaces (PES) and representative vibrational spectra. In this case, the vibrational spectra obtained from theoretical analysis are expected to indicate and identify modes of interest, but they are not expected to reproduce or fully describe all the spectral features obtained experimentally. We consider the case of pure TDMAHf reacting with a fully hydrogenated Si−H* (100) surface, where hydrogen abstraction occurs by direct reaction of the Si−H with the Hf precursor, forming a reactive Si radical surface site. Our calculations predict a barrier of 16.8 kcal/mol for this abstraction reaction. While this process is not expected to be excluded, we postulate that an abstraction reaction will likely be more facile with some oxygen present, either in the form of isolated OH* groups on the surface or possibly as OH on the precursor itself, where the precursor has reacted with residual water vapor in the gas phase.[29] It is not unreasonable to expect some oxygen, most likely in the form of water, to be present in the reaction chamber during processing. Furthermore, it is likely that HF-last Si(100) will involve some surface OH groups because H_2O is present in most HF sources, including anhydrous mixtures, and H_2O is a product of HF and SiO_2. We therefore consider the case of hydrogen abstraction from Si−H sites on the dimerized Si(100) surface where the Si−H are initially on a dimer site with an isolated Si−OH unit.

To model the reaction pathway for the first ALD half-reaction (i.e., TDMAHf reaction with a hydrogen-terminated Si surface with isolated Si−OH sites), we consider two

(29) Fenno, R. D.; Halls, M. D.; Raghavachari, K. *J. Phys. Chem. B* **2005**, *109*, 4969−4976.

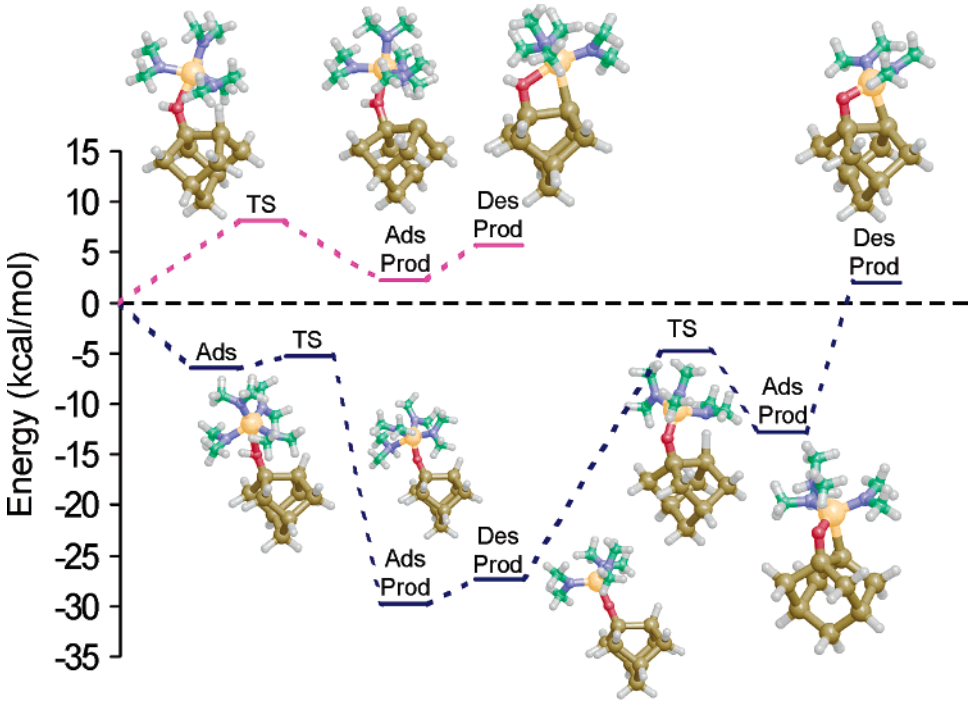

Figure 9. Potential energy surface for TDMAHf reacting with the silicon hydride surface adjacent to a Si−OH surface bond site. Two reaction pathways are depicted. The bottom pathway corresponds to reaction sequence (1 → 2) whereas the top pathway corresponds to sequence (2 → 1).

possible reactions involving OH groups: (1) the TDEAHf reacts with the isolated Si−OH* group through a hydrogen transfer to achieve a stable configuration and (2) the TDEAHf reacts at the isolated OH* site and abstracts a hydrogen atom from an adjacent Si−H* site, resulting in Si−H bond removal. These reaction steps could occur sequentially, producing the final product state that is independent of the reaction sequence. We therefore explore theoretically two pathways: pathway 1 → 2, where hydrogen is first transferred from the OH* to TDEAHf, followed by abstraction of neighboring hydrogen from Si−H* by the surface −O−Hf(L)$_3$* product, and alternately, pathway 2 → 1, where physisorption of TDMAHf on the Si−OH site occurs first, leading to H abstraction from adjacent Si−H*, followed by hydrogen transfer to the surface −Hf(L)$_3$* from the surface Si−OH* group. The reaction pathway (1 → 2) is written schematically as

$$\mathrm{Hf(L)_4 + Si{-}OH^* \rightarrow Si{-}O{-}Hf(L)_3 + H(L)_{(g)}}$$

$$\mathrm{Si{-}O{-}Hf(L)_3 + Si{-}H^* \rightarrow Si{-}O{-}Hf(Si)(L)_2 + H(L)_{(g)}} \quad (1 \rightarrow 2)$$

and pathway (2 → 1) can be written as

$$\mathrm{Hf(L)_4 + Si{-}OH^* \rightarrow Si{-}OH{-}Hf(L)_4^*}$$

$$\mathrm{Si{-}OH{-}Hf(L)_4^* + Si{-}H^* \rightarrow Si{-}OH{-}Hf(L)_3^* + H(L)_{(g)} + Si^*}$$

$$\mathrm{Si{-}OH{-}Hf(L)_3^* + Si^* \rightarrow Si{-}O{-}Hf(Si)(L)_2^* + H(L)_{(g)}} \quad (2 \rightarrow 1)$$

where (L) refers to the precursor dimethylamine ligand. Both pathways result in a four-membered Si−O−Hf−Si bonding structure that is expected to oxidize rapidly because of the high electron affinity of the Hf. We will show that on basis of the energetics of the reaction, the reaction pathway where reaction 1 precedes reaction 2 (i.e., pathway 1 → 2) will likely dominate.

We consider the case of TDMAHf reacting first with a surface hydroxyl group. The PES for this reaction pathway (pathway 1 → 2) for TDMAHf reacting with an OH* site on H-terminated Si(100)-2 × 1 (modeled by Si_9H_{13}−OH) is shown as the lower trace in Figure 9. In this case, TDMAHf first physisorbs at the Si−OH* site through a hydrogen-bonded state that is 6.4 kcal/mol lower in energy than the gas-phase reactant (labeled Ads in Figure 9). The adsorbed precursor then reacts by transferring the H of the surface Si−OH* through a transition state that is 1.2 kcal/mol above the H-bonded state. This leads to a product state that is 29.7 kcal/mol below the entrance channel, where Hf[N(CH$_3$)$_2$]$_3$* is bonded to the surface through a Si−O−Hf bridge, along with a dimethylamine (Ads Prod). Initially, the dimethylamine is bound to Hf through a dative bond, but it can readily desorb with an additional 2.4 kcal/mol (Des Prod). From this intermediate product (27.4 kcal/mol below the entrance channel), the surface Si−O−Hf[N(CH$_3$)$_2$]$_3$* can then abstract the neighboring Si−H* through a barrier that is 4.8 kcal/mol below the original entrance channel. This results in a dimethylamine that is dative bonded to the Hf atom (12.8 kcal/mol below the entrance channel) (Ads Prod). When the dimethylamine desorbs, the final product with two dimethylamine ligands on the Hf atom is formed, along with a Si−O−Hf bond and a direct Si−Hf bond (Des Prod). This final state is 2.0 kcal/mol above the original entrance channel. The energy for the desorption of the second dimethylamine is significantly larger than for the first, suggesting that residual dimethylamine may remain on the surface, necessitating a longer purge time or oxidant exposure time in the

ALD process. The surface Si−Hf bond is expected to readily undergo oxidation during water exposure in the second ALD half-reaction. The overall calculated energy change of ~2 kcal/mol for this first half-reaction is small, even at room temperature.

An alternative reaction pathway (pathway 2 → 1) can initiate by reaction with a neighboring surface Si−H bond, and the PES for this route is shown as the upper line in Figure 9. In this reaction scheme, the gas-phase precursor amine ligand abstracts a H atom from a neighboring Si−H* site without going through an initial physisorbed state, resulting in production of Si−OH−Hf[N(CH$_3$)$_2$]$_3$* where the Hf(L)$_3$ is dative bonded to the surface OH group. Again, hydrogen abstraction from the Si−H site by the N of the ligand leads to dimethylamine dative bonded to the Hf. Desorption of the dative-bonded dimethylamine byproduct leaves the dative bond between Hf and OH group intact and results in a Hf−Si bond involving the Si from which the H was abstracted. This abstraction route proceeds over a transition-state barrier of 8.2 kcal/mol relative to the gas-phase reactant, with the resulting Si−OH−Hf[N(CH$_3$)$_2$]$_3$* and adsorbed dimethylamine intermediate 2.2 kcal/mol above the energy of the reactants. Desorption of dimethylamine from this intermediate requires an additional 3.5 kcal/mol. Next, the H from the surface Si−OH* group could transfer to an alkylamine ligand via the four-centered ligand exchange reaction resulting in the elimination of a second dimethylamine ligand from the surface, forming the final product state. This product state is the same as for the pathway 1 → 2, where the Hf is linked to the surface through both a Si−O−Hf bridge and a Si−Hf bond.

The hydrogen transfer from the Si−OH* in pathway 2 → 1 requires a significant distortion in the electronic and geometric configuration of the surface species, and the transition state (not calculated) between the endothermic intermediate state (Si−OH*) and the final product state (Si−O−Hf−Si) becomes even less accessible at experimental temperatures. We conclude, therefore, that the surface reaction route which proceeds from 2 → 1 is not likely. For the direct abstraction route, the transition state is 16.8 kcal/mol above the entrance channel, whereas for the reaction pathway 1 → 2, the fully stabilized intermediate states are all endothermic relative to the starting state. This means that if the reactants are not thermally accommodated, residual energy can be available to help drive the reaction, effectively increasing the rate of reaction through pathway 1 → 2 as compared to the direct abstraction route. We conclude, therefore, that the reaction scheme that proceeds from 1 → 2 is the likely mechanism for Si−H* removal from hydrogen-terminated silicon surface during alkylamine precursor exposure.

Figure 10 shows the calculated vibrational spectra for the species involved in the calculated H transfer mechanism from the surface OH group. The first spectrum (bottom spectrum in the figure) shows the Si−H and O−H stretching modes of the initial surface at 2207 and 3880 cm^{-1}, respectively. After reaction with TDMAH via H transfer from the OH group, the OH modes disappear while the Si−H stretch remains and other modes of the adsorbed precursor appear.

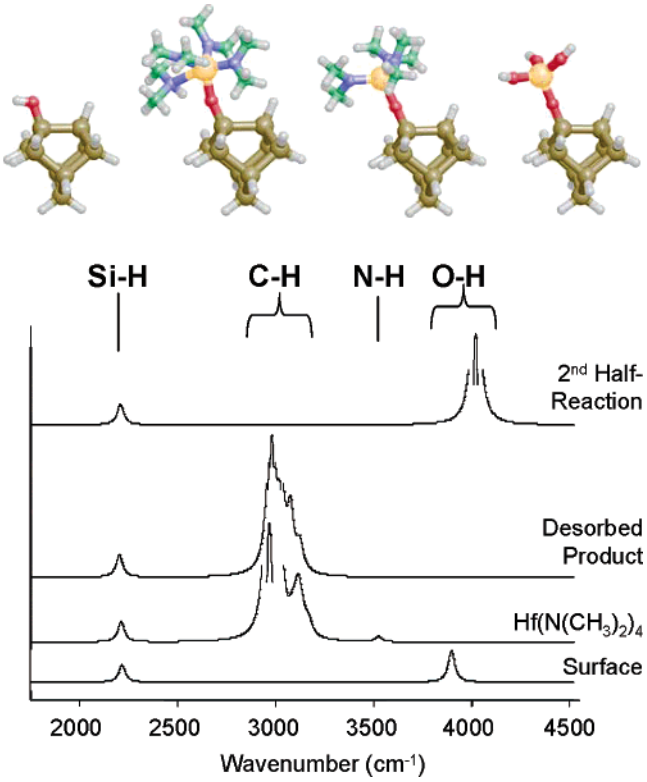

Figure 10. Calculated vibrational spectra for the species present in the H transfer process from the surface OH group. The reaction sequence shown at top (left to right) corresponds to the calculated spectra (bottom to top). The first spectrum (at bottom) shows the Si−H and O−H stretching modes of the initial surface at 2207 and 3880 cm^{-1}, respectively. After reaction with TDMAHf via H transfer from the OH group, the OH modes disappear while the Si−H stretch remains and other modes of the adsorbed precursor appear including the N−H stretch of the adsorbed product at 3512 cm^{-1}. The mode is not expected to be present after the product desorbs.

An NH mode is calculated at 3512 cm^{-1} from the dimethylamine byproduct that is dative bonded to Hf[N(CH$_3$)$_2$]$_3$*. Upon exposure of the Hf[N(CH$_3$)$_2$]$_3$* site to water, additional OH stretching modes appear as the amino ligand vibrational modes are removed.

Figure 11 shows the calculated vibrational spectra for the species involved in the calculated Si−H abstraction process. After reaction with TDMAH via H abstraction, the Si−H mode disappears while the other modes of the adsorbed precursor appear. The calculated results show an NH mode at 2916 cm^{-1}, which is significantly red-shifted from its typical range. This mode is only present when the dimethylamine byproduct is dative bonded to the surface. Upon exposure of the Hf[N(CH$_3$)$_2$]$_3$* site to water, additional OH stretching modes appear as the amino ligand vibrational modes are removed.

VI. Discussion and Conclusions

The experimental and theoretical results shown here give insight into the mechanisms and processes in hafnium alkylamine precursor adsorption and reaction on silicon oxide and hydrogen-terminated Si(100) surfaces. The data in Figure 4 is consistent with monolayer precursor adsorption on silicon oxide at low substrate temperatures, with incomplete removal of C−H containing ligands upon exposure to water vapor. Similar experiments for TDEAHf exposure on oxide surfaces

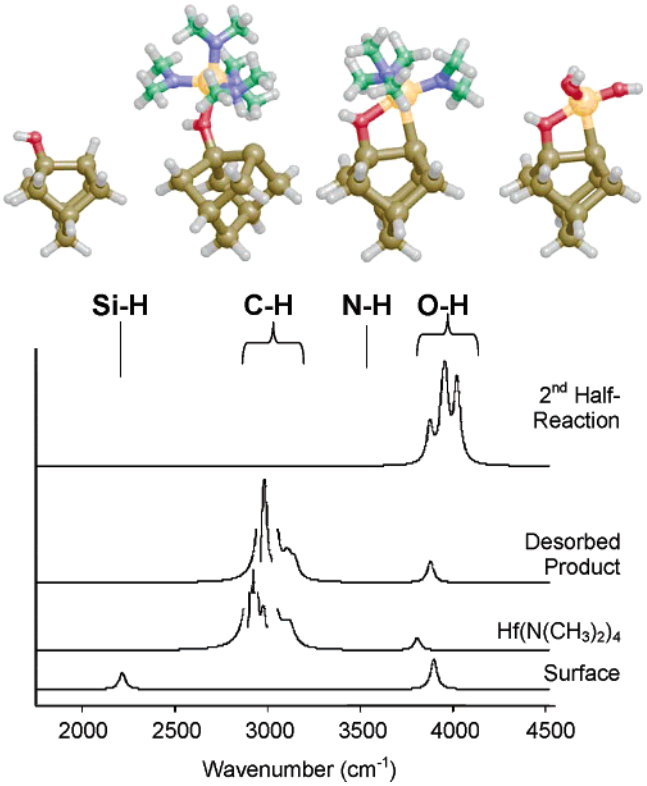

Figure 11. Calculated vibrational spectra for surface species in the Si−H abstraction process. The reaction sequence shown at top (left to right) corresponds to the calculated spectra (bottom to top). The first spectrum (at bottom) shows the Si−H and O−H stretching modes of the initial surface at 2207 and 3880 cm^{-1}, respectively. After reaction with TDMAH via H abstraction, the Si−H mode disappears while the other modes of the adsorbed precursor appear. For the adsorbed product, the N−H stretch has been shifted to 2916 cm^{-1} because of interactions with the bare surface Si atom. This peak is not observed after the product desorbs.

at temperatures between 150 and 250 °C show less C−H absorbance, with a small reduction upon exposure to water vapor. Because of the high sensitivity of the TDEAHf to water vapor, some reaction between the precursor and ambient or physically absorbed water could proceed before the IR analysis. Also, changes in OH related features are difficult to interpret in the experimental system used, in part because of the broad width of the absorption band expected for associated surface OH and because the surface OH density is sensitive to temperature and vacuum conditions for both the reference starting surface and the subsequent analyzed film. Precursor uptake on SiO_2 is also expected to be less than on HfO_2 surfaces because of differences in the nature and stability of reactive intermediates in these reactions.

It is important to note a significant distinction between physisorption of hafnium alklyamines on Si−OH surfaces (i.e., growth initiation on silicon oxide) versus on Hf−OH surfaces (i.e., growth continuation on hafnium oxide). For TDMAHf on the Si−OH surface, the dative-bonded complex initially formed between the precursor and surface Si−OH* site is bound by ∼6 kcal/mol, whereas the same precursor dative bonded to Hf−OH* sites is much more stable (∼20 kcal/mol). This is because the precursor metal center has four Hf−N sigma bonds and four Hf−N $d_\pi-p_\pi$ bonds which results in a fully occupied d-shell. This full shell does not allow formation of dative bonds between Hf and the lone pairs of the surface Si−OH* sites and so the precursor forms an adduct that is hydrogen bonded to the surface OH. However, on Hf−OH*, an amine ligand in the precursor can more readily break its $d_\pi-p_\pi$ bond with the precursor metal because it can form a dative bond to a surface metal atom which acts as the Lewis acid, allowing the precursor metal atom to also act as a Lewis acid and dative bond to the oxygen of the surface OH. In the reactions considered above, after the N atom of the amine ligand removes H from either Si−H* or Si−OH*, the Hf center then accepts electron density from the O atom of the surface OH site to form a stable Hf−O bond. Because the hydrogen-bonded precursor on Si−OH* is significantly less stable than the dative-bonded precursor to Hf−OH*, this reaction does not involve intermediates that are as strongly trapped as on HfO_2. Furthermore, the barrier to ligand exchange with the Si−OH* site is insignificant. Consequently, we expect that most reactions at isolated Si−OH* sites will proceed initially through hydrogen transfer from Si−OH*. This is entirely exothermic relative to the entrance channel. However, the difference between Si−OH* and Hf−OH* in the initial precursor adsorption energy indicates that the chemisorption reaction probability at isolated Si−OH* sites will be lower than that at Hf−OH* sites.

Considering reactions on the Si−H* terminated surface, the data in Figures 6−8 indicate that precursor adsorption involves a hydrogen removal step and that the hydrogen removal continues over many precursor/water exposure cycles. Several different mechanisms could allow for hydrogen abstraction. For example, in the case of trimethyl aluminum exposure on Si−H* surfaces, H abstraction is believed to proceed by direct formation of methane and dimethylaluminum bound to Si in an Al−Si linkage.[9] An analogous process for the hafnium alkylamine would result in formation of diethylamine and a Hf−Si bond, where three diethylamine ligands remained on the surface bound hafnium. This "direct" abstraction from Si−H* is not favorable because of the relatively large barrier of 16.8 kcal/mol for this pathway. Another possibility is the pathway described above, where the precursor adsorbs on reactive surface OH sites, followed by H abstraction from neighboring Si−H* sites by surface-bound alkylamine ligands. On the Si−H* starting surface, the OH density will normally be very low making the overall reactive sticking coefficient of the alkylamine also very low. This is consistent with the smaller intensity of surface C−H modes observed on the Si−H* surface as compared to the Si−OH* surface. After undergoing the H transfer processes described above, the remaining alkylamine ligands are available to remove H atoms from neighboring Si−H* surface sites. However, the removal of Si−H* is limited to those sites within reach of the N atom of the alkylamine adsorbed at what was initially an Si−OH* site. We believe, therefore, that the observed continuation in hydrogen removal occurs through the following mechanism. After the first half-reaction at the Si−OH* sites on the H-terminated silicon surface, the product surface is exposed to H_2O which readily reacts with the Hf−Si sites to create new Si−OH sites adjacent to existing Si−H sites. These new Si−OH/Si−H site pairs are then available to

undergo the reaction set described above, so that precursors from subsequent growth cycles continue to remove H from the surface at positions further removed from the initial OH nucleation site. This scheme, on the basis of our predicted reaction mechanisms, is consistent with the data in Figure 6 that shows that subsequent exposure of the surface to water and precursor cycles results in continuous loss of Si−H from the growth surface.

The detailed reaction processes in ALD of HfO_2 on Si−H terminated surfaces is important for high-dielectric constant gate insulators in advanced transistor devices, where well-defined reaction steps will be required to achieve submonolayer control of the Si/HfO_2 interface bonding structure. The results suggest that the hydrogen abstraction mechanism results in very reactive silicon radical or Si−Hf sites at the dielectric/insulator interface. These sites subsequently oxidize during processing forming interfacial silicon oxide and possibly mixed $HfSiO_x$ bonds. Alternate growth schemes or precursor structures may eventually be preferred that control or limit hydrogen abstraction to achieve better control of this critical interface during dielectric processing.

Acknowledgment. This work was supported by NSF grant #0072784 and SRC/SEMATECH Front End Processing Center.

CM051064H